Electrically pumped silicon waveguide light sources

Hasitha Jayatilleka, Arsam Nasrollahy-Shiraz, and Anthony J. Kenyon*

Department of Electronic & Electrical Engineering, University College London, Torrington Place, London WC1E 7JE, UK

*t.kenyon@ee.ucl.ac.uk

Abstract: We report simulations of electrically pumped waveguide emitters in which the emissive layer contains silicon nanoclusters and erbium ions. Plasmonic coupling to metallic or semi-metallic overlayers provides enhancement of the radiative rate of erbium ions, enabling high quantum efficiency emission. Using 2D and 3D finite difference time domain (FDTD) simulations we show that up to 75% of the light emitted from the active layer can be coupled into a nanowire silicon rib waveguide. Our results suggest that such devices, which can readily be fabricated using CMOS processing techniques, pave the way for viable waveguide optical sources to be realized in silicon photonics.

OCIS codes: (130.3120) Integrated optics devices; (130.5990) Semiconductors; (230.7390) Waveguides, planar; (250.5300) Photonic integrated circuits.

References and links

1. M. Lipson, "Guiding, modulating, and emitting light on silicon-challenges and opportunities," J. Lightwave Technol. **23**(12), 4222–4238 (2005).
2. L. Pavesi, "Will silicon be the photonic material of the third millenium?" J. Phys. Condens. Matter **15**(26), R1169–R1196 (2003).
3. E. Purcell, "Spontaneous emission probabilities at radio frequencies," Phys. Rev. **69**, 681 (1946).
4. G. Ford and W. Weber, "Electromagnetic interactions of molecules with metal surfaces," Phys. Rep. **113**(4), 195–287 (1984).
5. K. Okamoto, I. Niki, A. Scherer, Y. Narukawa, T. Mukai, and Y. Kawakami, "Surface plasmon enhanced spontaneous emission rate of InGaN/ GaN quantum wells probed by time-resolved photoluminescence spectroscopy," Appl. Phys. Lett. **87**(7), 071102 (2005).
6. J. Vuckovic, M. Loncar, and A. Scherer, "Surface plasmon enhanced light-emitting diode," IEEE J. Quantum Electron. **36**(10), 1131–1144 (2000).
7. K. Saxena, V. Jain, and D. S. Mehta, "A review on the light extraction techniques in organic electroluminescent devices," Opt. Mater. **32**(1), 221–233 (2009).
8. M. Ramuz, L. Burgi, R. Stanley, and C. Winnewisser, "Coupling light from an organic light emitting diode (OLED) into a single-mode waveguide: Toward monolithically integrated optical sensors," J. Appl. Phys. **105**(8), 084508 (2009).
9. A. V. Zayats, I. I. Smolyaninov, and A. A. Maradudin, "Nano-optics of surface plasmon polaritons," Phys. Rep. **408**(3-4), 131–314 (2005).
10. E. Ozbay, "Plasmonics: merging photonics and electronics at nanoscale dimensions," Science **311**(5758), 189–193 (2006).
11. S. Wedge, J. Wasey, W. L. Barnes, and I. Sage, "Coupled surface plasmon-polariton mediated photoluminescence from a top-emitting organic light-emitting structure," Appl. Phys. Lett. **85**(2), 182 (2004).
12. W. L. Barnes, "Fluorescence near interfaces: the role of photonic mode density," J. Mod. Opt. **45**(4), 661–699 (1998).
13. O. Jambois, Y. Berencen, K. Hijazi, M. Wojdak, A. J. Kenyon, F. Gourbilleau, R. Rizk, and B. Garrido, "Current transport and electroluminescence mechanisms in thin SiO_2 films containing Si nanocluster-sensitized erbium ions," J. Appl. Phys. **106**(6), 063526 (2009).
14. O. Jambois, F. Gourbilleau, A. J. Kenyon, J. Montserrat, R. Rizk, and B. Garrido, "Towards population inversion of electrically pumped Er ions sensitized by Si nanoclusters," Opt. Express **18**(3), 2230–2235 (2010).
15. A. J. Kenyon, P. F. Trwoga, M. Federighi, and C. W. Pitt, "Optical properties of PECVD erbium doped silicon-rich silica—Evidence for energy transfer between silicon microclusters and erbium ions," J. Phys. Condens. Matter **6**(21), L319–L324 (1994).
16. M. Galli, D. Gerace, A. Politi, M. Liscidini, M. Patrini, L. Andreani, A. Canino, M. Miritello, R. L. Savio, A. Irrera, and F. Priolo, "Direct evidence of light confinement and emission enhancement in active silicon-on-insulator slot waveguides," Appl. Phys. Lett. **89**(24), 241114 (2006).

#154822 - $15.00 USD Received 19 Sep 2011; revised 21 Oct 2011; accepted 2 Nov 2011; published 16 Nov 2011

17. Y. Jun, R. Kekatpure, J. White, and M. Brongersma, "Nonresonant enhancement of spontaneous emission in metal-dielectric-metal plasmon waveguide structures," Phys. Rev. B **78**(15), 153111 (2008).
18. Y. C. Jun, R. M. Briggs, H. A. Atwater, and M. L. Brongersma, "Broadband enhancement of light emission in silicon slot waveguides," Opt. Express **17**(9), 7479–7490 (2009).
19. A. Hryciw, Y. C. Jun, and M. L. Brongersma, "Plasmon-enhanced emission from optically-doped MOS light sources," Opt. Express **17**(1), 185–192 (2009).
20. A. Hryciw, Y. C. Jun, and M. L. Brongersma, "Plasmonics: electrifying plasmonics on silicon," Nat. Mater. **9**(1), 3–4 (2010).
21. P. Horak, W. H. Loh, and A. J. Kenyon, "Modification of the Er^{3+} radiative lifetime from proximity to silicon nanoclusters in silicon-rich silicon oxide," Opt. Express **17**(2), 906–911 (2009).
22. R. J. Walters, R. V. A. van Loon, I. Brunets, J. Schmitz, and A. Polman, "A silicon-based electrical source of surface plasmon polaritons," Nat. Mater. **9**(1), 21–25 (2010).
23. R. Chance, A. Prock, and R. Silbey, "Lifetime of an emitting molecule near a partially reflecting surface," J. Chem. Phys. **60**(7), 2744 (1974).
24. A. D. Rakic, A. B. Djurisic, J. M. Elazar, and M. L. Majewski, "Optical properties of metallic films for vertical-cavity optoelectronic devices," Appl. Opt. **37**(22), 5271–5283 (1998).
25. N. Daldosso, D. Navarro-Urrios, M. Melchiorri, L. Pavesi, C. Sada, F. Gourbilleau, and R. Rizk, "Refractive index dependence of the absorption and emission cross sections at 1.54μm of Er coupled to Si nanoclusters," Appl. Phys. Lett. **88**(16), 161901 (2006).
26. J. Dionne, L. Sweatlock, H. Atwater, and A. Polman, "Plasmon slot waveguides: towards chip-scale propagation with subwavelength-scale localization," Phys. Rev. B **73**(3), 035407 (2006).
27. A. V. Krasavin and A. V. Zayats, "Silicon-based plasmonic waveguides," Opt. Express **18**(11), 11791–11799 (2010).
28. Y. A. Vlasov and S. J. McNab, "Losses in single-mode silicon-on-insulator strip waveguides and bends," Opt. Express **12**(8), 1622–1631 (2004).
29. J. Bao, N. Yu, F. Capasso, T. Mates, M. Troccoli, and A. Belyanin, "Controlled modification of erbium lifetime in silicon dioxide with metallic overlayers," Appl. Phys. Lett. **91**(13), 131103 (2007).
30. P. Worthing, R. Amos, and W. Barnes, "Modification of the spontaneous emission rate of Eu^{3+} ions embedded within a dielectric layer above a silver mirror," Phys. Rev. A **59**(1), 865–872 (1999).
31. R. Walters, J. Kalkman, A. Polman, H. Atwater, and M. de Dood, "Photoluminescence quantum efficiency of dense silicon nanocrystal ensembles in SiO_2," Phys. Rev. B **73**(13), 132302 (2006).
32. A. F. Oskooi, D. Roundy, M. Ibanescu, P. Bermel, J. D. Joannopoulos, and S. G. Johnson, "MEEP: A flexible free-software package for electromagnetic simulations by the FDTD method," Comput. Phys. Commun. **181**(3), 687–702 (2010).

1. Introduction

The lack of an efficient silicon-based optical source is the most pressing challenge facing silicon photonics. Silicon is an indirect band gap semiconductor and suffers from strong nonradiative decay processes—as a result it is a very inefficient light source. Nevertheless, a wide range of passive optical devices such as filters, modulators and detectors have been demonstrated on silicon optical platforms using silicon-on-insulator (SOI) technologies [1]. There are many close-to-market applications driving this research, the leaders being optical interconnect technology, telecommunications (particularly the enablement of fiber-to-the-home) and lab-on-a-chip devices. Further into the future, photonics is well placed to deliver quantum computing, optical data storage, and a range of novel biophotonics technologies. The immediate and pressing requirement to push photonics technology into the mainstream is for a monolithic silicon light source [2].

It is well known that luminescent active materials placed within microstructures that support dense optical modes exhibit enhanced spontaneous emission rates due to Purcell effects [3,4]. This phenomenon has already been exploited to create efficient Light Emitting Diodes (LEDs), using InGaN/GaN quantum dots [5,6] and organic compounds [7,8]. The luminescent active material in these devices was placed between electrode layers in the form of sub-100nm thick films, increasing decay rates by emitting into Surface Plasmon Polariton (SPP) modes [9–12].

We have previously investigated electroluminescence from erbium-doped silicon-rich silica (SiO_x) [13,14], a material that has been of considerable interest since the demonstration of sensitization of erbium luminescence by excitation transfer from silicon nanoclusters [15]. This is a very appealing material for the fabrication of light emitting devices as it has the potential to overcome the limitations of silicon as an optical material while retaining CMOS processing compatibility. Recently, due to Purcell enhancement, a five-fold increase in emission from erbium doped silicon nanoclusters were observed in silicon slot waveguides

#154822 - $15.00 USD Received 19 Sep 2011; revised 21 Oct 2011; accepted 2 Nov 2011; published 16 Nov 2011

[16]. Theoretical investigations on CMOS compatible metal-dielectric-metal (MDM), metal-dielectric-semiconductor (MDS) waveguiding structures have demonstrated significant rate enhancements even at wavelengths around 1535nm, well away from the plasmonic resonances of the metallic layers [17–20].

Moreover, a further Purcell enhancement of the radiative emission rate of erbium ions is produced by their proximity to silicon nanoclusters in the oxide matrix [21]. Therefore, the possibility of fabricating a silicon-based electrically pumped waveguide optical source with a high quantum efficiency is an appealing one [22]. Here we present an analysis of such structures based on the metal-dielectric-semiconductor-dielectric (MDSD) geometry [19].

The device structure is illustrated in Fig. 1. A silicon rib waveguide sits on top of an oxide layer that provides optical and electrical isolation from the underlying silicon substrate. On top of this is a thin layer of erbium-doped silicon-rich silica (Er:SiO_x), on top of which is an electrode, which may be metallic (e.g., silver) or semi-metallic (e.g., indium tin oxide, ITO). Electrical contact to the electrode and silicon layers is provided by metallization, which is shown only schematically on the figure. The structure may readily be fabricated using silicon-on-insulator (SOI) wafers, allowing the waveguide layer to be single crystal silicon. This allows the waveguide losses to be minimized.

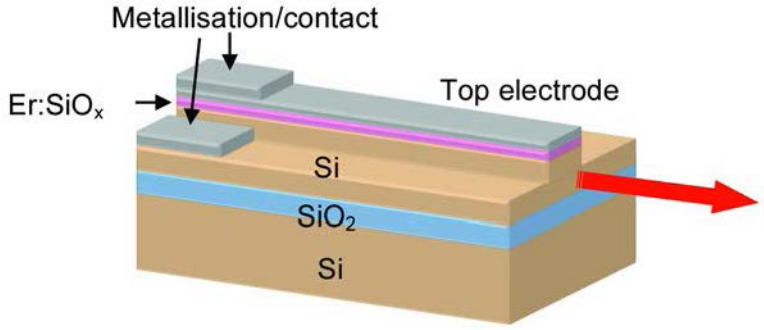

Fig. 1. Schematic of the emissive device structure

2. Enhancement of emission rates

We begin our analysis by investigating how the decay rates of emitters, specifically erbium in the SiO_x system, are modified when embedded in MOS structures. A cross-section of an MDSD structure such as that in Fig. 1 is shown in Fig. 2.

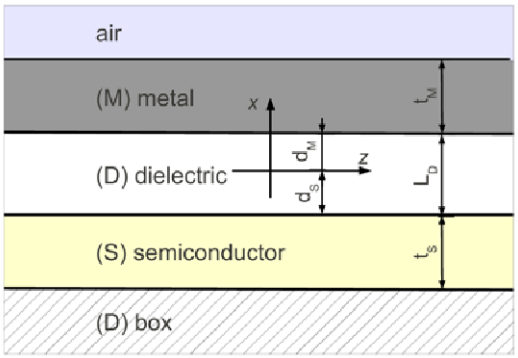

Fig. 2. Cross-section of an MDSD structure. The same structure was used to analyze MDM and MDS geometries by replacing the semiconductor and the dielectric layers in the lower half plane with semi-infinite metal and semiconductor layers.

#154822 - $15.00 USD Received 19 Sep 2011; revised 21 Oct 2011; accepted 2 Nov 2011; published 16 Nov 2011

The changes in erbium decay rates can be evaluated using the dipole approximation derived in [4,12,23]. We consider a dipole located at the origin of the coordinates shown in Fig. 2—that is, at the center of the dielectric layer. The normalized decay rate of the dipole under investigation, with respect to a dipole located far from any interface, is given by

$$\hat{\gamma} = 1 - \eta + \eta \int_0^\infty \frac{1}{P_{free}} dp \frac{dP}{dp} \tag{1}$$

Where η is the internal quantum efficiency of the dipole, P the classically dissipated power, and p the in-plane wavevector. Considering the magnitude of the wavevector in the dielectric ($k_D = 2\pi\varepsilon_D^{1/2} / \lambda_0$), the out of plane wavevector, $q_D = \left(k_D^2 - p^2\right)^{1/2}$, the dipole orientation vector ($|\vec{\mu}|^2 = \mu_\perp^2 + \mu_\parallel^2$) and the modification to the electric field at the dipole ($A_{\perp,\parallel}^{P,S}$), the integrand in Eq. (1), can be evaluated to be

$$\frac{1}{P_{free}} \frac{dP}{dp} = \frac{3}{2} \frac{1}{k_D^3} \mathrm{Re}\left\{ \frac{p}{q_D} \left[\frac{\mu_\perp^2}{|\vec{\mu}|^2} p^2 A_\perp^P + \frac{1}{2} \frac{\mu_\parallel^2}{|\vec{\mu}|^2} \left(k_D^2 A_\parallel^S + q_D^2 A_\parallel^P \right) \right] \right\} \tag{2}$$

where

$$A_\perp^P = \frac{\left[1 + r_{dma}^P \exp\left(2iq_d d_m\right)\right]\left[1 + r_{dsb}^P \exp\left(2iq_d d_s\right)\right]}{\left[1 - r_{dma}^P r_{dsb}^P \exp\left(2iq_d L_D\right)\right]} \tag{3}$$

$$A_\parallel^S = \frac{\left[1 + r_{dma}^S \exp\left(2iq_d d_m\right)\right]\left[1 + r_{dsb}^S \exp\left(2iq_d d_s\right)\right]}{\left[1 - r_{dma}^S r_{dsb}^S \exp\left(2iq_d L_D\right)\right]} \tag{4}$$

$$A_\parallel^P = \frac{\left[1 - r_{dma}^P \exp\left(2iq_d d_m\right)\right]\left[1 - r_{dsb}^P \exp\left(2iq_d d_s\right)\right]}{\left[1 - r_{dma}^P r_{dsb}^P \exp\left(2iq_d L_D\right)\right]} \tag{5}$$

In our notation, superscripts P and S refer to the parallel polarized magnetic field (TM) and the parallel polarized electric field (TE). Subscripts $\perp$ and $\parallel$ denote the perpendicular and parallel orientations of the dipole, respectively, and subscripts a, m, d, s, b are used to indicate the order of the dielectric stack (air-metal-dielectric-semiconductor-dielectric) as shown in Fig. 1. $r_{dma}^{P,S}$ and $r_{dsb}^{P,S}$ refer to the reflection coefficients calculated by applying Fresnel's equations towards the slab components in $x+$ and $x-$ directions from the dipole. We consider the perpendicular and the parallel orientations for the dipoles separately to obtain the decay rates $\hat{\gamma}_\perp$ and $\hat{\gamma}_\parallel$. Assuming that the dipoles are isotropic, these rates are combined to give the average normalized decay rate [12]:

$$\hat{\gamma} = \frac{1}{3}\hat{\gamma}_\perp + \frac{2}{3}\hat{\gamma}_\parallel \tag{6}$$

Figure 3(a) and (b) show the power spectrum (the result of Eq. (2) and the normalized decay rates of a dipole located in the middle of a 20nm thick dielectric layer in MDM, MDS and MDSD waveguide stacks. In all cases we have used silver [24] as the metal and silicon as the semiconductor material. Where necessary, the dielectric constant of the medium with the emitters is taken to be 2.25, approximating that of erbium doped silicon-rich silica [25], and the dielectric constant of the buried oxide layer (box) is taken to be 2.074 (silica).

#154822 - $15.00 USD Received 19 Sep 2011; revised 21 Oct 2011; accepted 2 Nov 2011; published 16 Nov 2011

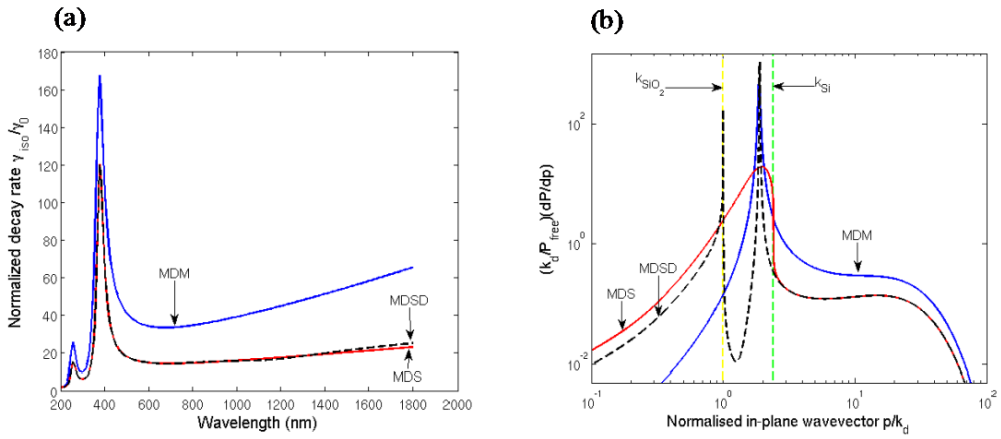

Fig. 3. (a) Power spectrum of MDM, MDS and MDSD waveguides at an emission wavelength of 1535nm. The light lines of Si and SiO_2 are shown in green yellow, respectively. (b) Enhancement factors for the different structures observed over a range of wavelengths. k_{Si} and k_{SiO2} indicate the light lines of silicon and silica, respectively.

According to Fig. 3, the rate enhancement obtained using the MDSD or MDS structure is considerably lower than that for an MDM waveguide. However, when used as an on-chip integrated device, a MDSD waveguide structure will have certain advantages over a MDM waveguide. As an example, reduced skin depth of the MDSD modes will reduce absorption losses [26,27]. Furthermore, as we demonstrate in the next section, the MDSD modes can be designed to have a very high mode overlap with low loss, high-index-contrast silicon nanowire waveguides [28], facilitating extremely efficient light coupling between the plasmonic and the photonic modes.

We next calculate the rate enhancement for a distribution of dipoles concentrated in the dielectric layer of an MDSD structure. We consider the dipole distribution along the $x-$axis to be $f(x)$, then the total luminescence intensity is written as a function of x and time (t) as

$$I(t)=\int f(x).\exp\left(-\hat{\gamma}(x)t\right)dx \qquad (7)$$

$I(t)$ may then be fitted with a stretched exponential function to obtain the averaged decay rates for the ensemble of emitters [29,30]. In Fig. 4 we plot the calculated decay rates for a

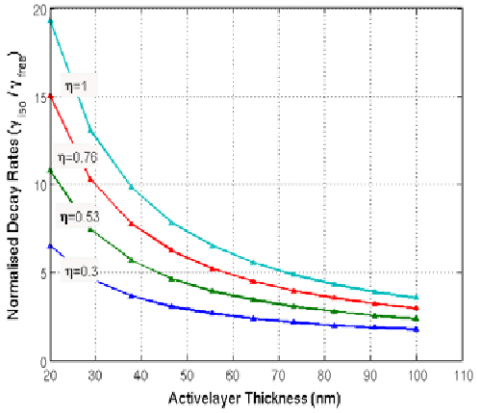

Fig. 4. Radiative rate enhancement of an ensemble of emitters in the dielectric layer of an MDSD structure (emission wavelength = 1535nm). The errors due to numerical integration and fitting of stretched exponential curves are too small to be indicated by error bars.

#154822 - $15.00 USD Received 19 Sep 2011; revised 21 Oct 2011; accepted 2 Nov 2011; published 16 Nov 2011

MDSD structure with different dielectric layer (active layer) thicknesses and a continuous distribution of emitters. The active layer is separated from the top Ag layer (150nm thick) by a 10nm spacer layer to avoid light coupling to lossy surface waves [4]. The calculated rate enhancements at a wavelength of 1535nm vary from ~13 for η=1 to ~7 for η=0.53, the latter being close to reported quantum efficiencies from silicon nanocluster based active material [31].

By integrating over the relevant poles of the power spectrum obtained from the emitter distribution (Fig. 5(a)), the power coupled into different decay channels (TE and TM modes, lossy waves, or radiation) as a function of the active layer width of the MDSD structure can be calculated. The results of such calculations are shown in Fig. 5(b). Significantly, 85% of the light emitted from the dipoles is coupled in to the TM mode for an active layer thickness of 30nm.

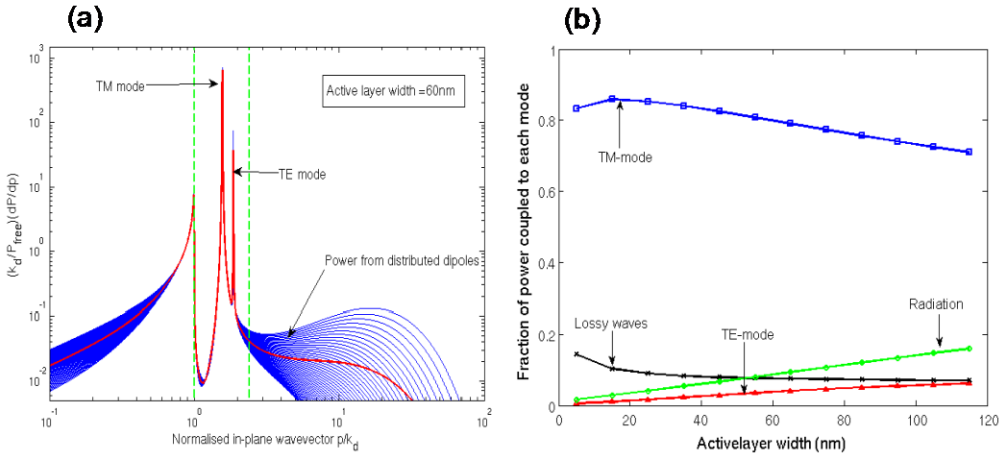

Fig. 5. (a) Average power dissipated into each mode (shown in red) from a uniform distribution of dipoles with arbitrary orientation. The blue lines represent the power dissipated from each dipole. The dashed green lines are the light lines of SiO_2 and Si. (b) Fraction of power from the emitters coupled in to each decay channel. Error bars are too small to be indicated.

3. Light coupling from active layer to silicon waveguide

3.1. 2D simulations

Initially, we used 2-dimensional FDTD simulations using a freely available software package (MEEP) [32] to investigate light coupling from the above analyzed MDSD waveguide to a low loss silicon nano-wire waveguide [28] for long range propagation. A diagram of the simulation space and the field intensity plot is shown in Fig. 6.

A line source placed across the height of the active layer was used to simulate the distributed emitters (erbium ions). Transmission and reflection were measured by line flux meters placed across the waveguides at either side of the device edge. The flux meter length was determined by separately evaluating the modal area incorporating more than 90% of the light propagating in infinitely long MDSD/silicon waveguide modes. A 2nm×2nm grid resolution was used in our simulations, which reduced the relative error by ~1.5% in transmission from a grid size of 4nm×4nm at a wavelength of 1535nm. The reduction in relative error obtained by further enhancing the resolution up to 1nm×1nm was less than 0.5%.

Figure 7 shows the calculated transmission, reflection and losses at the device edge as functions of active layer thickness and Si waveguide height. The length of the MDSD section was kept constant at 500nm.

#154822 - $15.00 USD Received 19 Sep 2011; revised 21 Oct 2011; accepted 2 Nov 2011; published 16 Nov 2011

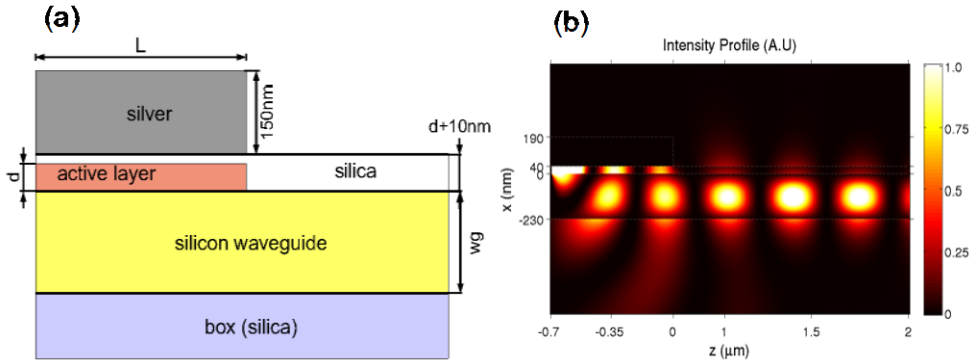

Fig. 6. (a) Diagram of the 2D FDTD simulation space (b) Light intensity plot obtained from FDTD simulations showing light coupling into a silicon waveguide near the MDSD and silicon waveguide interface.

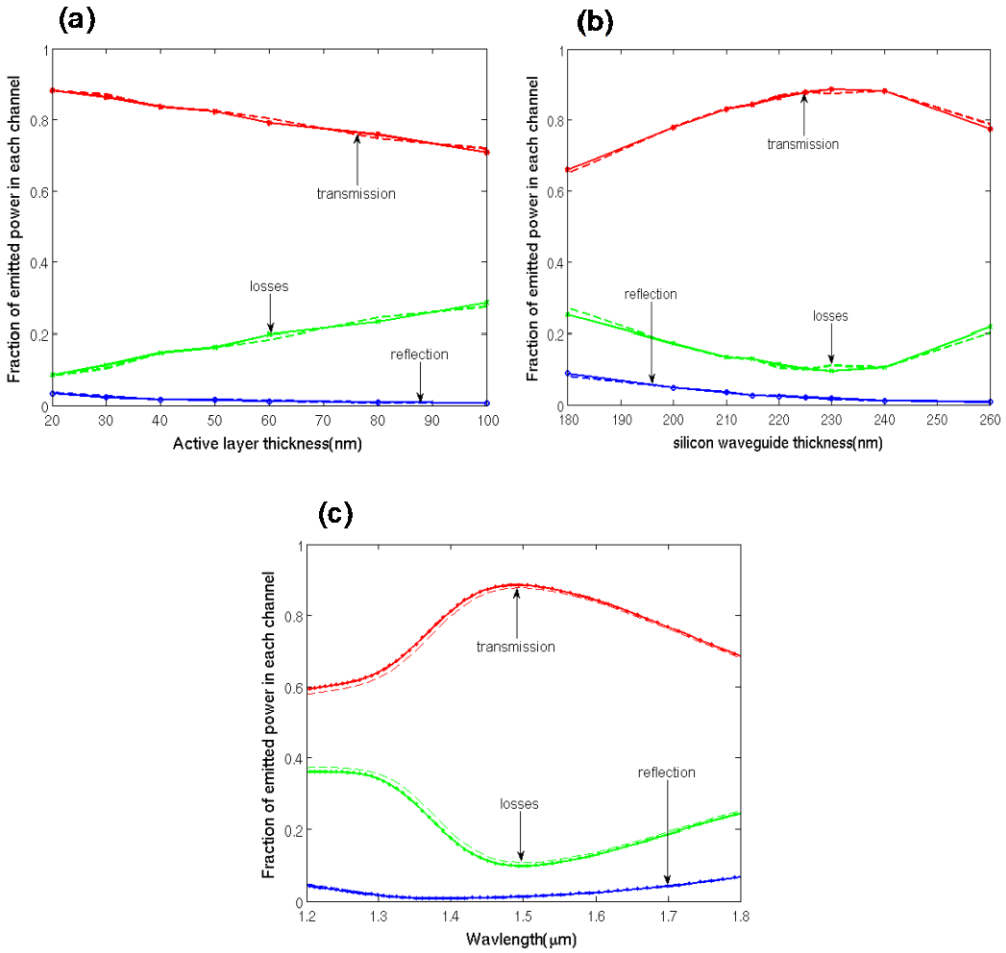

Fig. 7. Transmission, reflection and losses of the 2D geometry as a function of (a) active layer thickness (b) silicon waveguide thickness (height) (c) wavelength for the desirable structure (i.e., active layer thickness of 30nm and waveguide height of 230nm). The solid lines represent the results with a FDTD grid resolution of 2nm×2nm. The dashed lines represent the same simulation with a grid resolution of 4nm×4nm. The difference between the dashed and solid lines gives an indication of the errors in the simulation.

#154822 - $15.00 USD Received 19 Sep 2011; revised 21 Oct 2011; accepted 2 Nov 2011; published 16 Nov 2011

As observed from Fig. 7(a), the efficiency of coupling into the silicon waveguide reduces as the active layer thickness increases. Figure 7(b) was obtained for a constant active layer thickness of 30nm. The optimum height of the silicon waveguide was found to be ~230nm, at which point 88% of the 1535nm light in the MDSD waveguide is coupled into the silicon waveguide. The transmission, reflection and loss spectra near optical wavelengths for these device dimensions are shown in Fig. 7(c). It was also observed that increasing the MDSD device length improves the transmission efficiency, as this allows the light emitted in the active layer to be fully coupled to the MDSD modes before reaching the edge of the device.

3.2. 3D simulations

Considering the values obtained from the 2-D simulations, comparable coupling efficiencies (~89% transmission) were obtained for an optimized 3D device structure. The MDSD length of the simulated device was 600nm, coupling into a silicon nanowire waveguide with a width of 450nm and a height of 260nm (Fig. 8(a)).

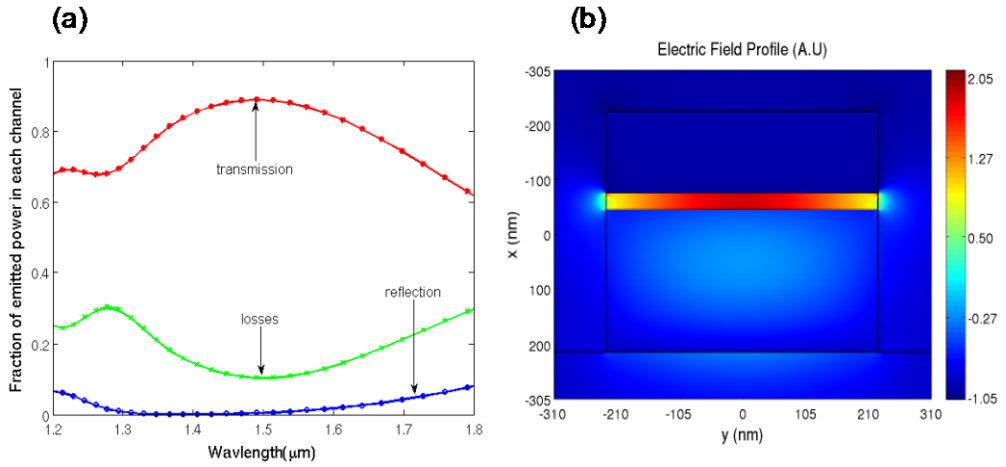

Fig. 8. (a) Transmission, reflection and loss spectrum for a desirable 3D device structure. (b) Electric field profile for the same 3D structure.

The electric field profile (Fig. 8(b)) of the TM mode for the optimized 3D structure was obtained using the method of Finite Elements using a commercially available software package. The effective index (n_{eff}) of the MDSD guided mode was found to be 2.49, and the attenuation coefficient was $5.57\text{x}10^{-2}\mu\text{m}^{-1}$. Therefore, a 600nm long device will only experience an attenuation of 0.145dB due to the absorption of the metallic contact.

4. Conclusion

An MDSD structure with a silver top contact, an active layer thickness of 30nm, silicon waveguide height of 260nm and a width of 450nm increased the decay rates of an ensemble of emitting erbium ions (η=0.53), by a factor of seven. 85% of the light emitted from the active layer was coupled in to the TM mode of the MDSD structure. For the above device dimensions, the MDSD TM mode has an n_{eff} of 2.49 and an attenuation coefficient of $5.57\text{x}10^{-2}$ μm^{-1}, indicating very low losses. FDTD simulations indicate that 88% coupling efficiencies at a wavelength of 1535nm are achievable between a 600nm long MDSD waveguide of the said dimensions and a silicon waveguide. Thus, 75% of the light generated in the active layer by electrical pumping can couple into the silicon waveguide beyond the electrical contacts. This can be a promising solution for silicon based emission technologies.

#154822 - $15.00 USD Received 19 Sep 2011; revised 21 Oct 2011; accepted 2 Nov 2011; published 16 Nov 2011